

# Strong Polarized Enhanced Raman Scattering via Optical Tunneling through Random Parallel Nanostructures in Au Thin Films

Alexandre G. Brolo,\* Erin Arctander, and Christopher J. Addison

Department of Chemistry, University of Victoria, P.O. Box 3065, Victoria, BC, Canada V8W 3V6

Received: September 1, 2004; In Final Form: October 15, 2004

Random parallel nanostructures (ridges and channels) were created by scratching gold thin films deposited on glass slides. Atomic force microscope (AFM) images showed that the width of the substructures within the scratches were of the order of a few hundred nanometers. These nanometric gold features can then support localized surface plasmon resonances in the direction perpendicular to the propagation of the scratches. This surface plasmon excitation led to a remarkable dependence of the intensity of the surface-enhanced resonance Raman scattering (SERRS) on the polarization direction of the incident light relative to the orientation of the scratch. The maximum SERRS intensities for oxazine 720 (a common laser dye) adsorbed on these nanostructures were obtained when the polarization of the light field was perpendicular to the direction of the substructures. The SERRS intensities followed a squared dependence on the polarization direction of the incident field.

## Introduction

The nanotech revolution is a direct consequence of the intriguing optical, electrical, and magnetic properties observed for materials in the nanometric length scale. Nanoparticles and nanostructures from noble metals are particularly interesting due to their ability to support direct excitation of surface plasmon (SP) modes in the optical range.<sup>1</sup> Surface plasmon polaritons (SPP) are extended electromagnetic waves which travel parallel to the surface. These modes cannot be created using direct monochromatic light incident from air onto a flat metallic surface due to a momentum mismatch.<sup>1</sup> This problem can be circumvented by providing optical excitation from a glass substrate (prism coupling) or by introducing periodic corrugations on the metal surface at the length scale of the wavelength of the incident light (grating coupling).<sup>1</sup> In either case, the conditions for creation of extended SP modes are achieved at specific angles where the parallel component of the  $k$ -vector of the incident photon matches the SP momentum for that specific excitation frequency.<sup>1</sup> Metallic nanoparticles and nanostructures support localized surface plasmon (LSP) resonances<sup>2</sup> which can be directly excited. These resonances are dependent on geometrical parameters and are mainly located at the tips, depressions, or junctions of the particles or nanostructures. All these SP resonances (SPPs and LSPs) are surface-confined, generating strong electromagnetic fields tightly located in a sub-wavelength region at the metal–dielectric interface. The light–SP interaction can then be controlled by tailoring the structure of the metal surface. These can potentially be applied for the generation of plasmonic circuits in miniaturized devices.<sup>3</sup>

The concentrated electric field from SP resonances is responsible for the enhanced spectroscopic signal observed in surface-enhancement Raman scattering (SERS).<sup>4</sup> SERS is among the most sensitive spectroscopic methods with limit of detection down to the single molecule level for some species.<sup>5,6</sup> Since SERS is a SP-mediated phenomenon, the magnitude of

the effect is highly dependent on the excitation conditions, nature, and geometry of the metallic nanostructures. Therefore, a vast variety of substrates have been used for SERS (spherical nanoparticles,<sup>7</sup> nanorods,<sup>8</sup> nanostructured electrode surfaces,<sup>9</sup> cold deposited films,<sup>10</sup> multilayered nanostructures,<sup>11</sup> organized metal islands,<sup>12</sup> and others<sup>4</sup>), and each of these substrates presents its own specific advantages and disadvantages in terms of reproducibility, sensitivity, detection limit, and cost. Here we show that surface-enhanced resonance Raman scattering (SERRS) of oxazine 720 dye can be obtained in transmission mode (forward scattering), using random sets of parallel nanostructures (channels and ridges) which are formed by scratching the surfaces of ultrathin gold films. The SERRS from this type of substrate showed a remarkable dependence on the polarization state of the incident beam, with a maximum efficiency obtained when the polarization vector of the incident field was perpendicular to the direction of the nanostructures. This polarization effect is reminiscent of the polarized transmission of white light through metallic nanowire gratings<sup>13</sup> and slits.<sup>14</sup>

Several ultrasensitive bioanalytical detection schemes that utilize enhanced Raman scattering have been demonstrated.<sup>15–17</sup> The polarization effect reported here offer an additional level of control that can be used in the design of complex biochips for multiplex analysis. Moreover, the polarization effect could also be explored beyond the realm of chemical analysis. For instance, nanophotonic devices that need polarization discrimination, such as optical switches, can be envisioned. An added advantage in this case is that the polarization effect is observed in the inelastic scattered radiation; therefore, the polarization-sensitive information can be easily isolated from the incident beam using an appropriate optical filter. Finally, the substrate used in this work does not require any special condition for patterning (such as vacuum systems); hence, it is very cost-effective.

## Experimental Section

The substrates (from evaporated metal films, EMF) were 100 nm thick gold films deposited on 1 in. × 1 in. glass slides. A

\* Corresponding author: Tel (250) 721 7167; Fax (250) 721 7147; e-mail: agbrolo@uvic.ca.

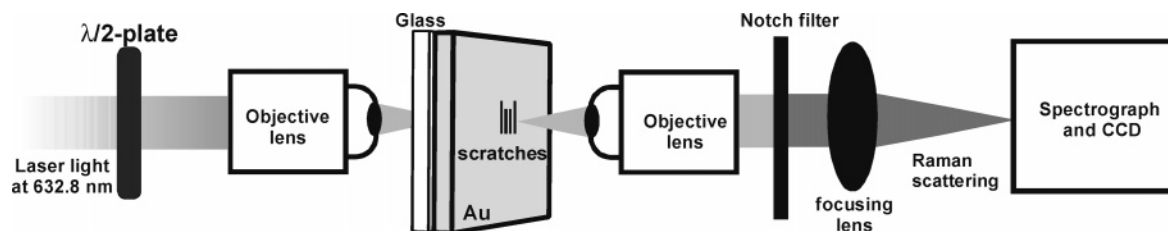


**Figure 1.** Experimental setup for forward Raman scattering. The direction of the polarized electric field for the light relative to the scratches is set by the half-wave plate ( $\lambda/2$  plate). The adsorbed molecule was at the gold–air interface, but the excitation was done from the glass side.

5 nm chromium layer was used to improve the adhesion of the gold to the glass. The randomly distributed nanostructures were prepared by mechanically scratching the Au films. Two scratching procedures were used, and both yielded strong polarized Raman signals in the forward scattering geometry. In the first procedure, a ca.  $10\ \mu\text{m}$  metallic tip was gently pressed against the surface and dragged parallel to two sides of the glass slide. The second procedure involved the use of fine emery paper to produce the scratches. In both procedures it was important to avoid completely scraping the gold off the surface. The main idea was to create a set of randomly distributed parallel gold lines or troughs at the surface of the gold film. This type of substructure would allow the evanescent field of an incident light from the glass side to tunnel through the gold film and excite the surface plasmons modes supported by the nanostructures.

The scratched surface was modified using a droplet evaporation procedure. In this case, a drop of  $10\ \mu\text{M}$  solution of oxazine 720 (from Lambdachrome) in HPLC grade methanol (Aldrich) was added to the surface. The solvent was allowed to evaporate, after which the surface was rinsed with a copious amount of ultrapure water ( $18.2\ \text{M}\Omega\ \text{cm}$ , from a Barnstead NANOpure Diamond water purification system). This procedure ensures that at most one monolayer of the adsorbate was present at the surface during Raman measurements.

Figure 1 shows the Raman instrumentation, which was modified from its conventional scattering arrangement ( $90^\circ$  geometry) to allow the spectral measurements in transmission mode (forward scattering). This experimental geometry guarantees that the amount of excitation at the gold–air interface will be directly related to the evanescent field and the surface plasmon excitation. A 35 mW He–Ne laser (from Melles Griot) at 632.8 nm was used as the excitation source. The laser was directed through a polarizer to ensure the polarization purity. Then, the polarized beam was passed through a half-wave plate mounted on a rotation stage. This arrangement allows the direction of the polarization vector to be rotated with regard to the main axis of the scratches. The laser light reached the sample from the glass side of the substrate, and it was focused through the scratches containing the nanostructures using a  $10\times$  Olympus microscope objective (numerical aperture = 0.25). The transmitted light (containing the Raman information) was collected using a similar microscope lens. The fundamental frequency (Rayleigh scattering) was rejected using a Kaiser super-notch filter, and the remaining radiation was directed through a Kaiser Holospec  $f/1.4$  spectrograph coupled with an Andor CCD detector (model DV-401-BV). The substrates and the optical components were mounted in mechanical stages that allow fine positioning control, and a wide-view microscope was used to aid the alignment of the incoming laser light with the scratches. The atomic force microscope (AFM) images were obtained using a Thermomicroscope Explorer SPM. All scans

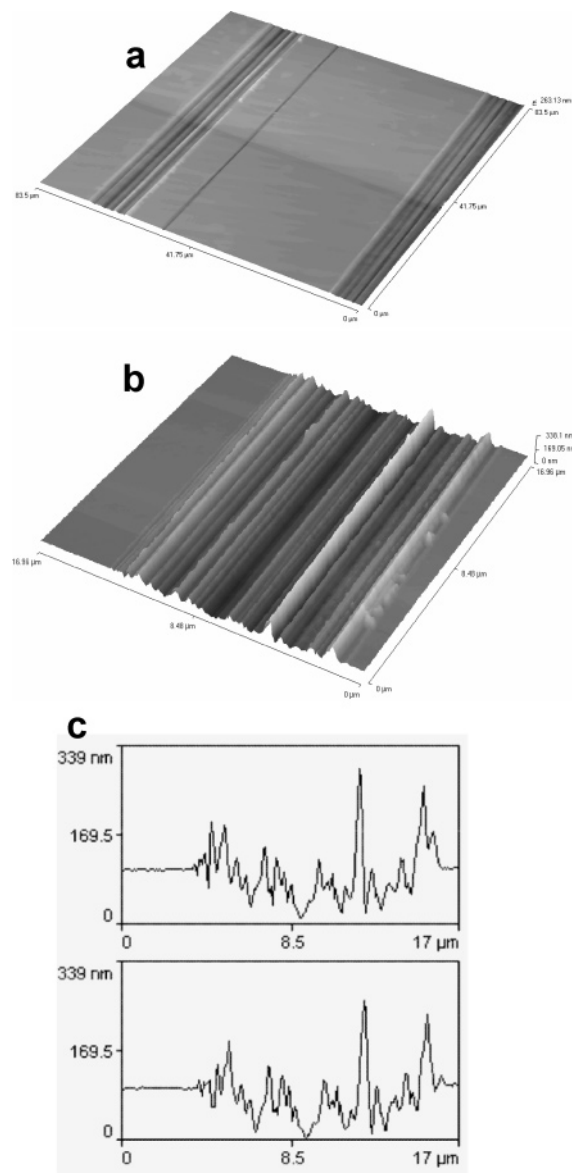


**Figure 2.** AFM images of the scratches. Scan ranges: (a)  $83.5 \times 83.5\ \mu\text{m}$ ; (b)  $17 \times 17\ \mu\text{m}$ . (c) Line scan along the scratch at two different positions in (b). All scans were obtained in noncontact mode at  $200\ \mu\text{m/s}$ . The resolution was 200 lines/scan.

were run in noncontact mode at  $200\ \mu\text{m/s}$ . The scan range and resolution were typically  $100\ \mu\text{m}$  and 200 lines/scan, respectively.

## Results and Discussion

Figure 2 shows typical AFM images of scratches on a 100 nm Au film, fabricated as described above. The total width of the scratches showed in Figure 2 is of the order of  $11\ \mu\text{m}$ . Figure 2a–c clearly indicates that a substructure is present within each

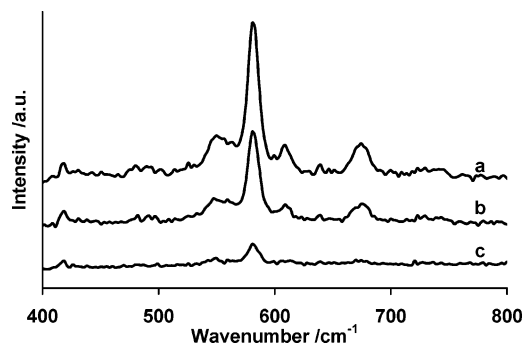


**Figure 3.** Enhanced Raman spectra obtained in the forward scattering geometry shown in Figure 1. The scratch was aligned along the  $z$ -axis. The axis and angles definitions are shown in Figure 4: (a)  $\Psi = 90^\circ$ ; (b)  $\Psi = 45^\circ$ ; (c)  $\Psi = 0^\circ$ .

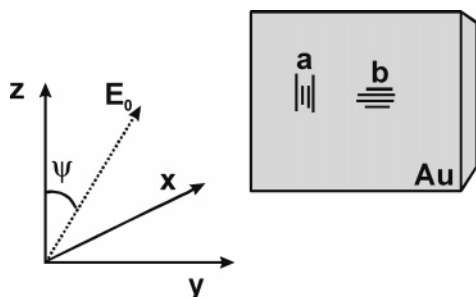


**Figure 4.** Definition of the coordinate system. The  $x$ -axis is the direction of propagation.  $E_0$  is the (polarized) electric field of the light.  $\Psi$  is the angle between the polarization and the defined  $z$ -axis.

scratch. The substructures are basically formed by a random set of parallel ridges and trenches of different geometric parameters (Figure 2). The line scans presented in Figure 2c are particularly informative. They demonstrate that within the scratch some gold was removed from certain regions creating channels (thinner than the original 100 nm). On the other hand, gold was also accumulated in other regions creating ridges (taller than the initial Au thickness). The lateral width of these nanostructures ranges between 200 and 800 nm. The line scans in Figure 2c present the same features and were obtained in two different regions perpendicular to the scratch in Figure 2b. This shows that the features run parallel to each other, and this parallelism is maintained in a long spatial range (on the micrometer scale).

It has been long recognized that the maximum enhancement of the local electric field in spheroids of noble metals originates from the region of the highest curvature.<sup>4,18</sup> Recent numerical calculation of the plasmon resonances for metallic nanowires with nonregular cross sections confirms this spatial localization of the electric field.<sup>19</sup> These calculations showed that the SP resonances are highly localized at the tips of the nanostructures; consequently, the number of SP resonances per nanowire increases as the overall symmetry of the particle's cross section decreases.<sup>19</sup> The sharp tips and narrow channels presented within the substructures in Figure 2 should be ideal for the production of highly localized SP resonances and, consequently, SERS.

Figure 3 shows the surface-enhanced Raman spectra from oxa dye adsorbed on the nanostructured gold surface (shown in Figure 2) obtained in the forward scattering geometry (using the experimental setup shown in Figure 1). The spectra in Figure 3a–c were recorded for three different directions of the electric field polarization. Figure 4 shows the definition of the direction of the light propagation and electric field orientation relative to the frame of the sample. The spectra in Figure 3 were obtained for scratches aligned parallel to the  $z$ -axis defined in Figure 4.

The main vibrational features of adsorbed oxa<sup>20,21</sup> are presented in all spectra in Figure 3, together with a remarkable dependence on the Raman intensity on the polarization direction of the incident laser. The oxa vibrational bands at 549, 585, and 672  $\text{cm}^{-1}$  can all be assigned to the movements of the phenoxazine ring of the dye. The enhanced Raman scattering of oxa shown in Figure 3 is similar to that observed from the spectra of oxa adsorbed on roughened silver surfaces under electrochemical conditions.<sup>20,21</sup> Oxa has an electronic absorption band around 620 nm;<sup>22</sup> hence, the enhanced spectra in Figure 3 contain contribution from charge-transfer processes in a resonance Raman-like effect (SERRS effect). The strongest enhanced Raman spectrum was obtained for  $\psi = 90^\circ$  when the direction of the electric field polarization was perpendicular to the main axis of the nanostructure (Figure 3a). On the other hand, the SERRS signal was minimized when the electric field of the incident laser was at  $\psi = 0^\circ$ , parallel to the nanostructures (Figure 3c). Figure 3b shows a spectrum obtained with the electric field component of the incident light polarized at  $45^\circ$  relative to the scratches. In this case, the strength of the Raman signal was intermediate between parts a and c of Figure 3. These results are in accordance with the polarization dependence calculated for the SERS from individual metallic nanowires<sup>19</sup> and from periodic silver structures (silver gratings).<sup>23</sup> In all these cases, the electrons in the conductor are only spatially confined in the nanometric range along the direction perpendicular to the main axis of the structures, and the surface plasmons can then only be excited when the polarization vector of the light field are oriented at the same direction.

The simple procedures for substrate preparation described in the Experimental Section led to sample-to-sample variability in the absolute SERRS intensities. On the other hand, the polarization effect was observed in all samples that contain parallel scratches. In fact, similar polarization behavior as in Figure 3 was obtained from samples prepared using different metallic tips and also when the half-wave plate in Figure 1 was substituted by a variable retardation plate.

The polarization effect can be best visualized in Figure 5 where the intensity of the 585  $\text{cm}^{-1}$  band of oxa is plotted against the angle  $\psi$  between the polarized electric field and the  $z$ -axis (defined in Figure 4). Two curves are presented in Figure 5a,b, corresponding to two scratches on the same gold substrate but perpendicular to each other (as schematically represented in Figure 4). These results were obtained by rotating the half-wave plate (shown in the experimental setup in Figure 1) and recording a SERS spectrum at every  $5^\circ$  of half-wave plate rotation. The components of the incident electric field in the  $z$ - and  $y$ - directions, defined in Figure 4, are then

$$\vec{E}_z(\omega_0) = \vec{E}_0(\omega_0) \cos \psi \quad (1)$$

$$\vec{E}_y(\omega_0) = \vec{E}_0(\omega_0) \sin \psi \quad (2)$$

Polarization-dependent SERS have been reported for dyes and proteins in the context of single molecules adsorbed on metallic aggregates.<sup>5,24–26</sup> It is well-known that the maximum enhanced field is concentrated in the cavities and junctions within the aggregates of nanoparticles of free electron metals.<sup>27,28</sup> Strong polarization dependence is observed for aggregates involving two colloidal particles, with the SERS signal maximizing when the incident polarization vector is parallel to the connecting axis. The SERS intensity of hemoglobin was measured at several polarization angles ( $\phi$ ) relative to the interparticle axis of Ag dimers.<sup>29</sup> This variation of the SERS intensity with polarization angles was well-described by a  $\cos^4$ -



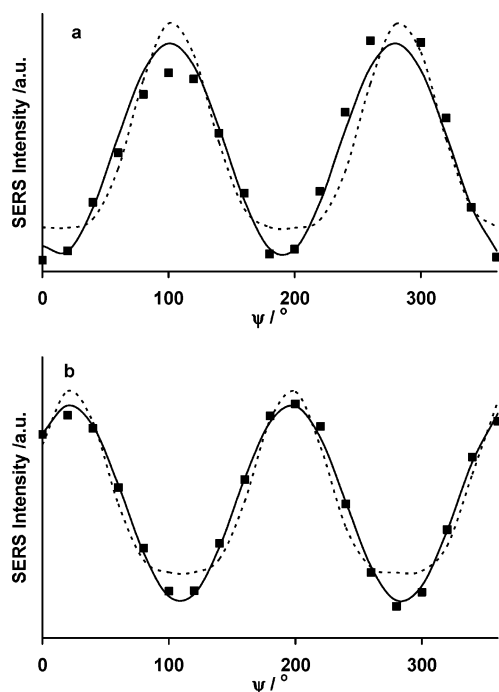


**Figure 5.** Polarization dependence of the intensity of the band at ca. 585  $\text{cm}^{-1}$  for two perpendicular scratches. (a) Scratch oriented along the  $z$ -axis (Figure 4). (b) Scratch oriented along the  $y$ -axis (Figure 4). The solid lines correspond to best fits using a sine (in (a)) and cosine (in (b)) squared functions. The dashed lines correspond to the best fit using  $\sin^4$  (in (a)) and  $\cos^4$  (in (b)) functions.

( $\phi$ ) dependency, which agreed well with a generalized Mie theory calculation.<sup>29</sup>

The most common models that account for SERS consider a polarizable dipole (molecule) adsorbed on a polarizable metallic sphere with dimensions smaller than the excitation wavelength (quasi-static condition). The field enhancement is proportional to the local field generated at the excitation laser frequency ( $E_{\text{local}}(\omega_0)$ ) and at the Raman scattered (Stokes) frequency ( $E_{\text{local}}(\omega_S)$ ). The SERS intensity ( $I_{\text{SERS}}$ ) is related to the square of the product of these fields at both the excitation and Raman-shifted frequency ( $E_0(\omega_0)$  and  $E_0(\omega_S)$ , respectively) normalized by the incident field, according to<sup>4</sup>

$$I_{\text{SERS}} \propto \left| \frac{E_{\text{local}}(\omega_0)}{E_0(\omega_0)} \frac{E_{\text{local}}(\omega_S)}{E_0(\omega_S)} \right|^2 \quad (3)$$

Since the energy of the Raman shifted photon is close to the energy of the exciting radiation, it is reasonable to consider that  $E_{\text{local}}(\omega_0) = E_{\text{local}}(\omega_S)$ , and the SERS intensity is proportional to the fourth power of the local field at  $\omega_0$ . In this case, a  $\cos^4(\phi)$  dependence of the SERS signal on the polarization is justifiable.<sup>29</sup> Similar polarization measurements were also reported for rhodamine 6G adsorbed on silver colloid aggregates, but in this case a  $\cos^2(\phi)$  dependence was observed.<sup>30</sup> The squared dependence can be rationalized by considering the different origins of  $E_{\text{local}}(\omega_0)$  and  $E_{\text{local}}(\omega_S)$ . While  $E_{\text{local}}(\omega_0)$  originates from the superposition of the incident field and the elastically Lorentz–Mie scattering,  $E_{\text{local}}(\omega_S)$  comes from the oscillating molecular dipole that radiates at the Raman frequency and the Raman-shifted scattered field.<sup>18,31</sup> The enhancement from  $E_{\text{local}}(\omega_S)$  is much more difficult to model than from  $E_{\text{local}}(\omega_0)$ .<sup>32</sup> In fact, only for the limit of a small spherical particles that the expressions for  $E_{\text{local}}(\omega_0)$  and  $E_{\text{local}}(\omega_S)$  are similar, and the approximation  $E_{\text{local}}(\omega_0) = E_{\text{local}}(\omega_S)$  is valid.<sup>32</sup> For more complex geometries, as the ones investigated in this work, these

local fields are not expected to be the same, and they might not follow the same polarization dependence. It is also unlikely that the orientation of the emission dipole at  $\omega_S$  is the same as the polarizable dipole  $\omega_0$ . Moreover, the molecules do not have one specific orientation and should be treated as a collection of incoherently dipoles. Under these circumstances, it is conceivable that the Raman shifted emission of the molecules should be isotropic (although the component of the emitting dipoles at the Raman frequency perpendicular to the main axis of the structure should excited the SP modes). Consequently, only the local field generated at  $\omega_0$  ( $E_{\text{local}}(\omega_0)$ ) would be directly related to the direction of the polarization of the incident light.

As discussed above, the only components of the incident electric field that can lead to surface plasmon resonances on parallel ridges and trenches are the ones perpendicular to the main axis of the elongated nanostructure.<sup>19,23</sup> Therefore, for a scratch positioned along the  $y$ -axis defined in Figure 4b, the  $z$ -component of the field ( $E_z$ ) will induce SP resonances with a local field ( $E_{z,\text{local}}$ ), and for a scratch positioned along the  $z$ -axis, only the  $y$ -component of the field is relevant ( $E_{y,\text{local}}$ ). Substituting eqs 1 and 2 into eq 3, we obtain the following angular dependence for the enhanced Raman signal for scratches aligned with the  $y$ -axis ( $I'$ ) and  $z$ -axis ( $I''$ ):

$$I' \propto |E_{\text{local}}(\omega_S) E_{\text{local}}(\omega_0) \cos \psi|^2 \quad (4)$$

$$I'' \propto |E_{\text{local}}(\omega_S) E_{\text{local}}(\omega_0) \sin \psi|^2 \quad (5)$$

The solid lines in Figure 5 correspond to the best calculated fit to the experimental data using sine- and cosine-squared functions for the  $z$ -oriented (Figure 5a) and  $y$ -oriented (Figure 5b) scratches, respectively. The dashed lines are the best fit using  $\cos^4 \psi$  and  $\sin^4 \psi$  functions. A better fit was obtained using the squared functions, in accordance with eqs 4 and 5. Despite the good agreement between eqs 4 and 5 and the experimental data, as observed in Figure 5, there are few aspects that need further consideration. First of all, small phase shifts (between 10 and 20 deg) were observed in all cases. This deviation may be simply attributed to the fact that the scratches were not perfectly parallel to the axis defined in Figure 4. Second, the SERS signal did not completely vanished for polarizations parallel to the major axis of the nanostructures. Moreover, the polarization effect observed here was not as strong as observed in experiments on the transmission of white light through an array of regularly arranged nanowires.<sup>13</sup> In that case, an extinction ratio of 26 was observed, and the maximum extinction ratio obtained from the SERS of molecules adsorbed on the parallel random structures in Figure 5 was of the order of 13. The residual Raman signal observed for polarization parallel to the nanostructures can be attributed to the randomness of the structure since some of the gold particles at the ridges and trenches may not follow the preferential orientation of the scratch. This residual Raman intensity has contributions from resonance Raman effects because the excitation energy used in these experiments (632.8 nm) was within the electronic absorption of oxa (ca. 620 nm). The contribution of electronic resonances on polarization effects observed in SERRS have been reported for single-wall carbon nanotubes adsorbed on silver colloids<sup>33</sup> and for pyromellitic dianhydride adsorbed on Cu-(100) and (111) single-crystalline surfaces.<sup>34</sup> In all these cases, however, the molecules assumed a well-defined orientation relative to the surface, and the mode-selective polarization dependence arises from the relative position between the incident electric field and the electronic transition dipole.<sup>34</sup> The random

nature of the substrate used in this work indicates that the oxa molecules will not have a unique long-range arrangement precluding any type of polarization dependence through the electronic resonances. On the other hand, this isotropic nature may allow a residual polarization-independent Raman signal, which would explain the Raman scattering observed for light polarization parallel to the major axis of the nanostructures.

White light transmission through the substructure was also measured for two polarization states (parallel and perpendicular to the scratches). A constant transmittance of less than 1% was observed at the far field throughout the entire visible spectrum, and no polarization dependence was observed (data not shown). This seems to indicate that the polarization dependence on the Raman signal was confined to the near field, affecting only the adsorbed molecules. The transmission of white light through sets of organized slits and nanowires are strongly polarized.<sup>19,35</sup> These structures also support a SP-mediated enhancement in the amount of transmitted light at certain frequencies. As can be seen in Figure 2, the gold was not completely removed from the substrate within the scratches. Gold is a very reflective substrate in the visible due to its negative dielectric constant in this optical range. Hence, the light field must tunnel through the remaining gold to reach the other side of the substrate. The SP-mediated evanescent transmission through a patterned thin Au thin film has been calculated using the 2-D finite-difference time-domain (FDTD) method.<sup>36</sup> Two transmission modes were discerned, one related to SPP and the other to LSP. Both modes were instrumental for the enhanced transmission of white light at certain frequencies. The LSP resonances, however, were broader and highly localized in the grooves of the grating structure.<sup>36</sup> On the basis of these results, we suggest that the evanescent field of the transmitted light excite LSP in the structures used in this work. These resonances do not present a defined peak in the white light transmission spectrum due to their broad characteristics and the random distribution of sizes and shapes within the substrate. The polarization dependence is only preserved in the near field, for species adsorbed on the nanostructures, because the far field is strongly contaminated with background evanescent radiation which tunnels through the very thin layer of the gold film.

## Conclusions

A set of parallel random structures, consisting of ridges and trenches of nanometric dimensions, have been created by scratching Au thin film substrates. Molecules of oxa dye adsorbed on these surfaces presented good quality surface-enhanced resonance Raman scattering (SERRS). The SERRS signal was strongly polarized, with maximum intensity obtained when the polarization vector of the incident light was perpendicular to the major axis of the nanostructures. The polarization dependence followed a square relationship with the longitudinal component of the incident field relative to the direction of the scratches. This polarization dependence was ascribed to the excitation of the LSP modes by the light field that tunnels through the Au thin film. Preferential transmission of polarized white light was not observed in the far field, indicating that this effect is mainly surface-sensitive and localized in the near-field range. The results presented here are the first report of polarization effects on the Raman scattering obtained in a

forward direction from parallel nanostructures. This polarization effect may add another degree of freedom on the application of Raman chips for bioanalytical chemistry, and it can also be used for the fabrication of switches in photonic devices.

**Acknowledgment.** We gratefully acknowledge funding support for this work from NSERC, CFI, BCKDF, and the University of Victoria.

## References and Notes

- (1) Raether, H. *Surface Plasmons on Smooth and Rough Surfaces and on Gratings*; Springer: Toronto, 1988.
- (2) Kelly, K. L.; Coronado, E.; Zhao, L. L.; Schatz, G. C. *J. Phys. Chem. B* **2003**, *107*, 668–677.
- (3) Barnes, W. L.; Dereux, A.; Ebbesen, T. W. *Nature (London)* **2003**, *424*, 824–830.
- (4) Moskovits, M. *Rev. Mod. Phys.* **1985**, *57*, 783–826.
- (5) Nie, S.; Emory, S. R. *Science* **1997**, *275*, 1102–1105.
- (6) Kneipp, K.; Wang, Y.; Kneipp, H.; Perelman, L. T.; Itzkan, I.; Dasari, R. R.; Feld, M. S. *Phys. Rev. Lett.* **1997**, *78*, 1667–1670.
- (7) Kneipp, K.; Kneipp, H.; Itzkan, I.; Dasari, R. R.; Feld, M. S. *Chem. Rev.* **1999**, *99*, 2957–2975.
- (8) Nikoobakht, B.; El-Sayed, M. A. *J. Phys. Chem. A* **2003**, *107*, 3372–3378.
- (9) Brolo, A. G.; Irish, D. E.; Smith, B. D. *J. Mol. Spectrosc.* **1997**, *405*, 29–44.
- (10) Seki, H. *J. Chem. Phys.* **1982**, *76*, 4412–4418.
- (11) Mulvaney, S. P.; He, L.; Natan, M. J.; Keating, C. D. *J. Raman Spectrosc.* **2003**, *34*, 163–171.
- (12) Duyne, R. P. V.; Hulteen, J. C.; Treichel, D. A. *J. Chem. Phys.* **1993**, *99*, 2101–2115.
- (13) Schider, G.; Krenn, J. R.; Gotschy, W.; Lamprecht, B.; Ditlbacher, H.; Leitner, A.; Aussenegg, F. R. *J. Appl. Phys.* **2001**, *90*, 3825–3830.
- (14) Takakura, Y. *Phys. Rev. Lett.* **2001**, *86*, 5601–5603.
- (15) Taton, T. A.; Mirkin, C. A.; Letsinger, R. L. *Science* **2000**, *289*, 1757–1760.
- (16) Graham, D. *Anal. Chem.* **2002**, *74*, 1069–1074.
- (17) Mulvaney, S. P.; Musick, M. D.; Keating, C. D.; Natan, M. J. *Langmuir* **2003**, *19*, 4784–4790.
- (18) Wang, D. S.; Kerker, M. *Phys. Rev. B* **1981**, *24*, 1777–1790.
- (19) Kottmann, J. P.; Martin, O. J. F.; Smith, D. R.; Schultz, S. *Phys. Rev. B* **2001**, *64*, 235402.
- (20) Brolo, A. G.; Sanderson, A. C.; Smith, A. P. *Phys. Rev. B* **2004**, *69*, 045424.
- (21) Brolo, A. G.; Sanderson, A. C. *Can. J. Chem.*, in press.
- (22) Schneider, S.; Grau, H.; Halbig, P.; Freunscht, P.; Nikel, U. *J. Raman Spectrosc.* **1996**, *27*, 57–68.
- (23) Kahl, M.; Voges, E. *Phys. Rev. B* **2000**, *61*, 14078–14088.
- (24) Bosnick, K. A.; Jiang, J.; Brus, L. E. *J. Phys. Chem. B* **2002**, *106*, 8096–8099.
- (25) Xu, H. X.; Bjerneld, E. J.; Kall, M.; Borjesson, L. *Phys. Rev. Lett.* **1999**, *83*, 4357–4360.
- (26) Jeong, D. H.; Zhang, Y. X.; Moskovits, M. *J. Phys. Chem. B* **2004**, *108*, 12724–12728.
- (27) Xu, H.; Aizpurua, J.; Kall, M.; Apell, P. *Phys. Rev. E* **2000**, *62*, 4318–4324.
- (28) Futamata, M.; Maruyama, Y.; Ishikawa, M. *Vib. Spectrosc.* **2004**, *35*, 121–129.
- (29) Xu, H.; Kall, M. *ChemPhysChem* **2003**, *4*, 1001–1005.
- (30) Itoh, T.; Hashimoto, K.; Ozaki, Y. *Appl. Phys. Lett.* **2003**, *83*, 2274–2276.
- (31) Kerker, M.; Wang, D. S.; Chew, H. *Appl. Opt.* **1980**, *19*, 4159–4173.
- (32) Schatz, G. C.; Duyne, R. P. V. In *Handbook of Vibrational Spectroscopy*; Chalmers, J. M., Griffiths, P. R., Eds.; Wiley: New York, 2002.
- (33) Kneipp, K.; Jorio, A.; Kneipp, H.; Brown, S. D. M.; Shafer, K.; Motz, J.; Saito, R.; Dresselhaus, G.; Dresselhaus, M. S. *Phys. Rev. B* **2001**, *63*, 081401.
- (34) Kambhampati, P.; Child, C. M.; Forster, M. C.; Champion, A. J. *Chem. Phys.* **1998**, *108*, 5013–5026.
- (35) Porto, J. A.; Vidal, F. J. G.; Pendry, J. B. *Phys. Rev. Lett.* **1999**, *83*, 2845–2848.
- (36) Liu, W.-C.; Tsai, D. P. *Phys. Rev. B* **2002**, *65*, 155423.